[CANCER RESEARCH 58, 3320–3330, August 1, 1998]

In Vitro and *in Vivo* Targeting of Immunoliposomal Doxorubicin to Human B-Cell Lymphoma[1]

Daniel E. Lopes de Menezes, Linda M. Pilarski, and Theresa M. Allen[2]

Department of Pharmacology, University of Alberta, Edmonton, Alberta, T6G 2H7 Canada [D. E. L. d. M., T. M. A.], and Department of Oncology, Cross Cancer Institute, Edmonton, Alberta, T6G 1Z2 Canada [L. M. P.]

ABSTRACT

The ability to selectively target liposomal anticancer drugs via specific ligands against antigens expressed on malignant cells could improve the therapeutic effectiveness of the liposomal preparations as well as reduce adverse side effects associated with chemotherapy. Long-circulating formulations of liposomes containing lipid derivatives of poly(ethyleneglycol) [sterically stabilized liposomes (SLs)] have been described previously, and new techniques have recently been developed for coupling monoclonal antibodies (Abs) at the poly(ethyleneglycol) terminus of these liposomes. Ab-targeted SLs [immunoliposomes (SILs)] containing entrapped anticancer drugs are predicted to be useful in the treatment of hematological malignancies such as B-cell lymphomas or multiple myeloma, in which the target cells are present in the vasculature.

The specific binding, *in vitro* cytotoxicity, and *in vivo* antineoplastic activity of doxorubicin (DXR) encapsulated in SILs coupled to monoclonal Ab anti-CD19 (SIL[anti-CD19]) were investigated against malignant B cells expressing CD19 surface antigens. Binding experiments with SIL[anti-CD19] resulted in a 3-fold higher association of the SILs with a human CD19$^+$ B lymphoma cell line (Namalwa) in comparison with nontargeted SLs. Using flow cytometry, fluorescently labeled SIL[anti-CD19] bound to B cells with no recognition of T cells in a mixture of B cells and T cells in culture. Nontargeted SLs demonstrated significantly lower recognition of either B cells or T cells. Targeted DXR-SIL[anti-CD19] displayed a higher cytotoxicity to B cells relative to DXR entrapped in nontargeted SLs.

Therapeutic experiments in severe combined immunodeficient mice implanted with Namalwa cells by the i.v. or i.p. routes resulted in significantly increased effectiveness of DXR-SIL[anti-CD19] compared to similar amounts of free DXR, DXR-SL (no Ab), or isotype-matched nonspecific Abs attached to DXR-SL. Single doses (3 mg/kg) of DXR-SIL[anti-CD19] administered i.v. resulted in a significantly improved therapeutic benefit, including some long-term survivors. From our results, we infer that targeted anti-CD19 liposomes containing the anticancer drug DXR may be selectively cytotoxic for B cells and may be useful in the selective elimination of circulating malignant B cells *in vivo*.

INTRODUCTION

B-cell malignancies (B-cell leukemias/lymphomas and MM[3]) remain a major group of human hematological cancers and are still largely incurable (1–4). Their immunological features and clinical prognosis are dependent on the malignant expansion of a clonal B-cell phenotype, and the diseased cells are confined mainly in the vascular compartment. Most patients initially respond to conventional chemotherapy and/or radiotherapy, but in nearly all cases, the disease recurs and becomes refractory to further treatment.

Recent therapeutic approaches to cancer have focused on developing novel delivery systems to increase the therapeutic indices of anticancer agents by targeting drugs to diseased cells and away from normal tissues (5). One approach uses the expression of cell surface epitopes as unique targets for the selective delivery of Ab-based therapies (*i.e.*, immunoconjugates, radiolabeled Abs, Ab-polymer conjugates, or immunoliposomes; Refs. 6–14). Liposome encapsulation of anticancer drugs can alter their pharmacokinetics and biodistribution, resulting in increased efficacy and/or decreased toxicity (15–19). Long-circulating dose-independent liposome formulations containing engrafted PEG on their surface (SLs or Stealth liposomes) have been developed (20–24), and DXR-containing SL (Doxil) has been approved in a number of countries for treatment of Kaposi's sarcoma (25).

With the recent development of methods for coupling specific ligands to the PEG terminus of SL (26–31), new opportunities exist for the use of liposomes as homing devices for selective targeting of anticancer drugs to diseased cells (13, 14, 32–36). Numerous studies have shown that SILs have significantly increased target cell binding *in vitro* (30–32, 34, 36) and result in improved therapeutic efficacy *in vivo* in the treatment of early (micrometastatic) solid tumors (14, 33). However, SILs seem to lose their advantage in treating more advanced solid tumors (14), likely because the binding site barrier restricts penetration of the SILs into the tumor interior (37, 38).

Targeting of immunoliposomes within the vasculature, where the SILs should have unrestricted access to malignant cells, is a feasible strategy for the treatment of hematological diseases (*e.g.*, B-cell or T-cell malignancies and MM). In particular, this strategy may allow selective eradication of the malignant B-cell population from the blood of B-cell lymphoma or MM patients. Selective targeting of the malignant B cells may have the additional advantage of preventing nonspecific toxicity to T cells, preserving T-cell-mediated immune responses in patients. An additional advantage might come from the ability of the SILs to overcome MDR in B cells (39–41). Targeting an internalizing CD19 epitope may result in enhanced delivery of the liposome-drug package to the cell interior, bypassing the plasma membrane MDR pump mechanism.

The CD19 receptors are exclusively expressed on most B-lineage malignancies and are absent on hematopoietic stem cells in the bone marrow (42, 43). This approach allows targeting to the malignant cells, leaving the progenitor population intact. The free anti-CD19 Ab, by itself, has cytotoxic effects and is currently in preclinical and clinical trials for the therapy of B-cell leukemias and lymphomas, conjugated to toxins or as targeted radiotherapy (43–49).

In this study, we selectively targeted CD19$^+$ malignant B cells *in vitro* and *in vivo* with DXR-containing SIL coupled with mAb anti-CD19 (DXR-SIL[anti-CD19]). A CD19$^+$ human B-cell lymphoma (the Namalwa cell line) that grows readily in SCID mice was chosen

Received 9/16/97; accepted 6/2/98.

The costs of publication of this article were defrayed in part by the payment of page charges. This article must therefore be hereby marked *advertisement* in accordance with 18 U.S.C. Section 1734 solely to indicate this fact.

[1] Supported by The Medical Research Council of Canada, Canada (UI-12411), SEQUUS Pharmaceuticals, Inc. (T. M. A.), and the National Cancer Institute of Canada with funds from the Canadian Cancer Society (L. M. P.).

[2] To whom requests for reprints should be addressed, at Department of Pharmacology, University of Alberta, Edmonton, Alberta, T6G 2H7 Canada. Phone: (403) 492-5710; Fax: (403) 492-8078; E-mail: terry.allen@ualberta.ca.

[3] The abbreviations used are: MM, multiple myeloma; PEG, poly(ethyleneglycol); SL, sterically stabilized liposome; SIL, sterically stabilized immunoliposome; Ab, antibody; mAb, monoclonal Ab; DXR, doxorubicin; MDR, multidrug resistance; SCID, severe combined immunodeficient; HSPC, hydrogenated soy phosphatidylcholine; DSPE, distearoylphosphatidylethanolamine; PEG_{2000}-DSPE, PEG (M_r 2000) covalently linked to DSPE; HZ, hydrazide-derivatized; CHOL, cholesterol; NBD-PE, 12-[*N*-(nitrobenz-2-oxa-1,3-diazol-4-yl)amino]dodecanoylphosphatidylethanolamine; MTT, 3-(4,5-dimethylthiazol-2-yl)-2,5-diphenyltetrazolium bromide; FBS, fetal bovine serum; [^{3}H]CHE, cholesteryl-(1,2-[^{3}H)(N)]-hexadecyl ether; TI, tyraminylinulin; FACS, fluorescence-activated cell sorting; PhE, phycoerythrin; PL, phospholipid; IF, immunofluorescence; MST, mean survival time; K_d, dissociation constant; MRT, mean residence time; $t_{1/2}$, blood half-life; AUC, area under the curve.

as a model system to examine liposome targeting. In these experiments, we demonstrate increased targeting and specific cytotoxicity to Namalwa cells by DXR-SIL[anti-CD19] relative to DXR-SL or free DXR. In addition, *in vivo* pharmacokinetics and survival experiments were performed in SCID mice xenografts of the Namalwa cell line. Our results demonstrate that targeted immunoliposomal therapy compared with either DXR-SL, free DXR, or free Ab can result in a significantly improved therapeutic benefit in mice implanted with the B-cell tumor.

MATERIALS AND METHODS

Materials. HSPC, PEG_{2000}-DSPE, and HZ-PEG-DSPE were generous gifts from SEQUUS Pharmaceuticals, Inc. (Menlo Park, CA) and have been described elsewhere (21, 29). CHOL and NBD-PE were purchased from Avanti Polar Lipids (Alabaster, AL). *N*-Acetyl-methionine, Sephadex G50, Sepharose CL-4B, sodium periodate, and MTT were purchased from Sigma Chemical Co. (St. Louis, MO). DXR (Adriamycin) was obtained from Adria Laboratories, Inc. (Mississauga, Ontario, Canada). RPMI 1640 and FBS was purchased from Life Technologies, Inc. (Burlington, Ontario, Canada). [^{3}H]CHE (1.48–2.22 TBq/mmol) was purchased from DuPont New England Nuclear (Mississauga, Ontario, Canada). Iodobeads were from Pierce Chemical Co. (Rockford, IL). TI synthesis and preparation of ^{125}I-TI have been described previously (50). All other chemicals were of analytical grade purity.

Mice. Female CD1(ICR)BR outbred mice were obtained from Charles River Laboratories (St. Constant, Quebec, Canada) and kept in standard housing. Female 4–6-week-old C.B.-17/Icr-Tac-SCID mice weighing 18–20 g were purchased from Taconic Farms (German Town, NY). The SCID mice were housed and maintained in sterile enclosures under specific virus and antigen-free conditions. SCID mice were maintained on a specified diet with trimethoprim-sulfamethoxazole in their drinking water. Mice were used when they were 7–10 weeks old. All experiments were approved by the Animal Welfare Committee of the University of Alberta (Edmonton, Alberta, Canada).

Cell Lines and Abs. Murine mAb anti-CD19 (from FMC-63 murine CD19 hybridoma) and isotype-matched control IgG2a (IAG0.11) were obtained from Dr. H. Zola (Children's Health Research Institute, Adelaide, Australia; Ref. 51). The concentration of all mAbs was determined by spectrophotometry (λ = 280 nm), and purity was assessed by SDS-PAGE. All mAb reactivities were checked before use by indirect IF using FITC-labeled goat antimouse Ab and FACS (Becton Dickinson, San Jose, CA) against appropriate cell lines. To discriminate individual populations of B and T cells in FACS experiments, the following mAb-fluorescent conjugates were used: (*a*) FMC63-FITC (anti-CD19-FITC conjugate); (*b*) B1RD1 (anti-CD20-PhE-conjugate; Coulter, Hialeah, FL); and (*c*) Leu-3-PhE (anti-CD4-PhE conjugate; Becton Dickinson) along with the appropriate FITC- or PhE-conjugated isotype-matched controls. Anti-CD45-PhE was mAb 17G10 from Dr. J. Wilkins (University of Manitoba, Winnipeg, Manitoba, Canada).

For iodination of the mAb, 2 mg of mAb in 300 μl of 25 mM HEPES and 140 mM NaCl (pH 7.4) were treated with 185 MBq of $Na^{125}I$ and 5 iodobeads in a 2-ml reaction vial at 22°C for 1 h. The resulting ^{125}I-labeled mAb was desalted over a Sephadex G25 column in the same HEPES buffer.

The human B-cell lymphoma line Namalwa (ATCC CRL 1432) was obtained from American Type Culture Collection (Rockville, MD). A human T-cell lymphoma line (H9; ATTC HTB 176) was a gift from Dr. L-J. Chang (Department of Medical Microbiology and Immunology, University of Alberta, Edmonton, Alberta, Canada). All cell lines were grown as suspension cultures in RPMI 1640 supplemented with 10% heat-inactivated FBS and maintained at 37°C in a humidified incubator (90% humidity) containing 5% CO_2.

Preparation of Liposomes. Liposomes were composed of either HSPC:CHOL:PEG_{2000}-DSPE at a 2:1:0.1 molar ratio of PLs or HSPC:CHOL:HZ-PEG_{2000}-DSPE at a 2:1:0.1 molar ratio. For fluorescently labeled liposomes, NBD-PE (1 mol% of PL) was incorporated into the lipid mixture. For ^{125}I-TI-loaded liposomes, the aqueous-space label was added during liposome hydration. In some experiments, [^{3}H]CHE was added as a nonmetabolized, nonexchangeable lipid tracer (52, 53). Briefly, dried lipid films were hydrated in 25 mM HEPES and 140 mM NaCl buffer (pH 7.4) and sequentially extruded (Lipex Biomembranes Extruder, Vancouver, British Columbia, Canada) through a series of polycarbonate filters (Nuclepore Corp., Pleasanton, CA) with pore sizes ranging from 0.4–0.08 μm. This extrusion procedure has been shown to produce primarily small unilamellar vesicles (54, 55). The mean diameter of liposomes was determined by dynamic light scattering using a Brookhaven B190 submicron particle size analyzer (Brookhaven Instruments Corp., Holtsville, NY). The diameters of extruded liposomes were in the range of 110 ± 10 nm.

For DXR-loaded liposomes, the drug was encapsulated by remote loading using an ammonium sulfate gradient (56). Briefly, liposomes were hydrated in 155 mM ammonium sulfate (pH 5.5), and the external buffer was exchanged by eluting through a Sephadex G50 column equilibrated with 123 mM sodium citrate (pH 5.5). DXR was added to the liposomes at a PL:DXR ratio of 1:0.2 (w/w) and incubated for 1 h at 65°C. The liposome-encapsulated DXR was separated from the free DXR over a Sephadex G50 column eluted with 123 mM sodium citrate (pH 5.5). The concentration of the liposome-entrapped DXR was determined by spectrophotometry (λ = 490 nm), and PL concentrations were determined using the Bartlett colorimetric assay (57). The loading efficiency of DXR was greater than 95%, and liposomes routinely contained DXR at a concentration of 140–160 μg DXR/μmol PL (0.24–0.28 μmol DXR/μmol PL).

SILs were prepared by the hydrazide coupling method (31). Briefly, mAb was oxidized with sodium periodate (10 mM in distilled water) for 1 h at 22°C. The excess periodate was quenched with 50 mM *N*-acetyl-methionine, and oxidized mAb was incubated with HZ-PEG-liposomes overnight at 5°C at an Ab:PL molar ratio of 1:1000. Finally, the immunoliposomes were separated from the free mAb over a Sephadex CL-4B column equilibrated with 25 mM HEPES (pH 7.4). The efficiency of coupling was determined from the amount of ^{125}I-labeled mAb bound to the surface of liposomes, expressed as μg mAb/μmol PL. All mAb coupling densities on liposomes (HSPC:CHOL:HZ-PEG_{2000}-DSPE, 2:1:0.1 molar ratio; 100 nm in diameter) were routinely in the range of 40–60 μg anti-CD19/μmol PL ($2.6–3.9 \times 10^{-4}$ μmol mAb/μmol PL).

***In Vitro* Cell Binding/Uptake Experiments.** Cell binding and uptake experiments were performed with Namalwa cells and H9 cells. Cells were plated at 1×10^6 cells/100 μl RPMI 1640 supplemented with 10% FBS in 48-well tissue culture plates. Various formulations of [^{3}H]CHE-labeled liposomes, with or without coupled anti-CD19, were added to each well (50–1600 nmol/ml) and maintained at either 4°C or 37°C in a humidified atmosphere containing 5% CO_2 in air in a total volume of 200 μl. In competition experiments, liposome binding was conducted in the presence of 6–200-fold excess free Ab (6.4×10^{-4} μmol of free anti-CD19) that was added 15 min before the addition of SIL[anti-CD19]. After a 1-h incubation, the cells were washed three times with cold PBS (pH 7.4), and the amount of [^{3}H]CHE-liposomes associated with the cells was determined by scintillation counting (Aqueous Counting Scintillant scintillation fluid) in a Beckmann LS-6800 counter. The amount of liposomes bound (in nmol PL) was calculated from the initial specific activity of [^{3}H]CHE-liposomes.

In some experiments, immunoliposomes were labeled with a green fluorescent lipid marker, NBD-PE (0.1 mol% of PL), and liposome-cell recognition was determined using FACS. Various formulations of NBD-PE-labeled liposomes were incubated with a mix of B and T lymphoma cells (1×10^6 cells/well) at a final PL concentration of 400 nmol/ml for 1 h at 37°C in a humidified incubator containing 5% CO_2. Cells were washed three times with IF buffer (PBS containing 0.1% FBS and 0.02% sodium azide) and fixed with 1% formaldehyde before analysis on the flow cytometer. Cell debris were excluded by appropriate gating on forward *versus* side angle scatter profiles. Files were collected of 10,000–20,000 events and later analyzed using the LYSIS II software program (Becton Dickinson). For two-color IF experiments with a mix of B and T lymphoma cells, cells were labeled with red-labeled anti-CD20-PhE (B-cell marker) or anti-CD4-PhE (T-cell marker) to identify the individual cell populations, in addition to the green-labeled liposomes. Appropriate fluorescent isotype control Abs were used to ascertain specific labeling and identify appropriate cell types.

***In Vitro* Cytotoxicity Experiments.** A comparison of the *in vitro* cytotoxicity of free drug and various liposomal formulations was performed on $CD19^+$ Namalwa cells and on a $CD19^-$ T lymphoma cell line (H9) with an *in vitro* proliferation assay using MTT (58). Briefly, 5×10^5 cells were plated in 96-well plates and incubated with either free DXR or various formulations of DXR encapsulated in long-circulating liposomes with or without Ab. Groups

included free anti-CD19, free isotype-matched IgG2a, free DXR (not liposome-entrapped), DXR-SL, and DXR-SL conjugated to anti-CD19 (DXR-SIL[anti-CD19]). DXR-SL and DXR-SIL were used alone or in conjunction with free anti-CD19 (10 μg/10^6 cells). Additional experiment groups included nonspecific isotype-matched IgG2a mAb (DXR-NSIL[IgG2a]) or empty (no DXR) SIL[anti-CD19]. Cells were incubated for 1, 24, or 48 h at 37°C in an atmosphere of 95% humidity and 5% CO_2. At the 1 and 24 h time points, the cells were washed twice before replacing with fresh media and incubated for an additional 47 and 24 h, respectively. All plates were incubated for a total of 48 h. At the end of the incubation time, tetrazolium dye was added, and the plates were read on a Titertek Multiskan Plus (Flow Laboratories, Inc., Mississauga, Ontario, Canada) at dual wavelengths of 570 and 650 nm.

Pharmacokinetic and Biodistribution of Liposomes in CD1(ICR)BR (Outbred) *versus* SCID Mice Implanted with CD19$^+$ Namalwa Cells. Female CD1(ICR)BR (outbred) mice or SCID mice bearing i.p. Namalwa cells in the weight range of 20–30 g were injected via the tail vein with a single bolus dose of 0.2 ml of liposomes (0.5 μmol PL/mouse). Liposomes were composed of HSPC:CHOL:HZ-PEG_{2000}-DSPE (2:1:0.1 molar ratio; 100 nm in diameter), with or without coupled anti-CD19 (or isotype-matched IgG2a), and contained approximately 2–4 × 10^5 cpm of aqueous-space label ^{125}I-TI (50, 59). At selected time points (0.5, 1, 2, 4, 6, 12, 24, or 48 h) postinjection, mice (three mice/group) were anesthetized with halothane and sacrificed by cervical dislocation. A blood sample (100 μl) was collected by heart puncture, and major organs (namely, the liver, spleen, lung, heart, and kidney) were excised. For tumor-bearing SCID mice, in addition, the mesenteric lymph nodes were isolated. All organs were counted for the ^{125}I label in a Beckmann 8000 gamma counter. Blood correction factors were applied to all samples (60). Pharmacokinetic parameters were calculated using polyexponential curve stripping and the least squares parameter estimation program PKAnalyst (Micromath, Salt Lake City, UT).

***In Vivo* Therapeutic Experiments.** Namalwa cells were passaged i.p. in SCID mice to develop a more virulent strain with reproducible tumor takes. The preadapted cell line was grown in tissue culture, and cells were harvested in sterile PBS. Cell viability was assessed by dye exclusion using eosin staining before implantation. SCID mice were injected with preadapted cells in 0.2 ml of sterile PBS either i.p. (5 × 10^7 cells) or i.v. via the tail vein (5 × 10^6 cells). Mice injected i.p. developed ascitic tumors and had a MST of 23 days. Mice injected i.v. had a MST of approximately 20 days, and mice were sacrificed when they showed signs of hind leg paralysis. From some mice, blood samples were taken by tail vein bleeding, and the blood lymphocytes were separated using Ficoll-Paque gradients. Deceased animals were subjected to a gross histopathological examination to detect tumor dissemination. To detect tumor cells in the tissues, samples of liver, spleen, lung, heart, kidney, bone marrow, and solid tumors were dissociated with Pronase-collagenase treatment, followed by labeling with both anti-CD19-FITC and anti-CD45-PhE, and analyzed by FACS.

For therapeutic experiments, mice (five mice/group) implanted with cells i.v. (5 × 10^6 or 1 × 10^5 cells) or i.p. (5 × 10^6 or 5 × 10^7 cells) were treated at either 1 or 24 h after implantation with single doses or three weekly doses of 3 mg/kg DXR (i.v. or i.p.) as either free DXR, DXR-SL (no Ab), DXR-SIL[anti-CD19], or DXR-NSIL[IgG2a]. Free mAb treatments (anti-CD19 or isotype-matched control IgG2a) were also investigated at doses of 10 μg/mouse. The contribution to the therapeutic results of the free mAb, anti-CD19, was investigated in conjunction with either free DXR, DXR-SL (no Ab), or DXR-SIL[anti-CD19]. Treatments were given as either a single dose or three weekly treatments at a dose of 3 mg/kg DXR. Mice were monitored routinely for weight loss, and survival times were noted.

Statistical Analysis. All linear regression analyses were done using Quattro Pro 4.0 (Borland, Inc., Scotts Valley, CA). Student's *t* test was used to measure statistical significance. Multiple comparisons of MSTs of various treatment groups were performed using ANOVA with INSTAT (GraphPAD software, version 1.11a). Data were considered significant for Ps < 0.05.

RESULTS

***In Vitro* Recognition Experiments.** To examine whether immunoliposomes (SIL[anti-CD19]) could specifically target CD19$^+$ B cells, *in vitro* binding studies were conducted at 4°C and 37°C with the Namalwa cell line and a control CD19$^-$ T-cell line (H9) (Fig. 1, *A–C*). Binding was quantified from the specific activity of [^{3}H]CHE counts associated with the cells. To discriminate the processes of cell binding and uptake, the experiments were conducted at 4°C and 37°C. The association (binding and uptake) of SIL[anti-CD19] or SL (no mAb) by 1 × 10^6 Namalwa cells after a 1-h incubation at 37°C is shown in Fig. 1*A*. There was a 3-fold increase in association of SIL[anti-CD19] to Namalwa cells compared to that of Ab-free liposomes (Fig. 1*A*). Binding/uptake of the SIL[anti-CD19] increased linearly at low lipid concentrations (50–200 nmol PL/ml) and seemed to saturate at concentrations greater than 400 nmol PL/ml (Fig. 1*A*). Association of SIL[anti-CD19] with Namalwa cells could be compet-

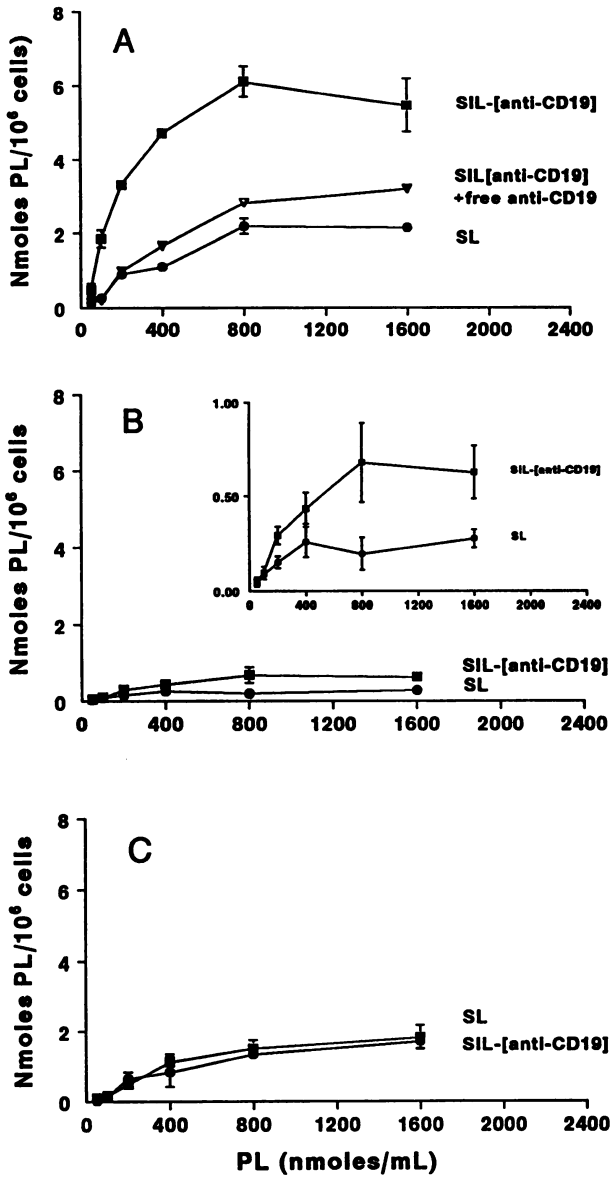

Fig. 1. Binding/uptake of [^{3}H]CHE-labeled liposomes by B cells and T cells as a function of liposome concentration. Liposomes were composed of HSPC:CHOL:PEG_{2000}-DSPE (2:1:0.1 molar ratio; 100 nm in diameter) ± mAb anti-CD19. SL or SIL[anti-CD19] was incubated with 1 × 10^6 Namalwa cells at either 4°C or 37°C. In competition experiments, the binding of SIL[anti-CD19] was conducted in the presence of excess free anti-CD19. *A*, Namalwa cells, 37°C; *B* (including the *insert*), Namalwa cells, 4°C; *C*, H9 cells, 37°C. Data are expressed as nmol PL ± SD/10^6 cells (n = 3).

itively inhibited by the addition of excess free anti-CD19, indicating that the association was mediated through the CD19 surface epitope on B cells (Fig. 1*A*). Nonspecific binding/uptake of SL (no Ab) was also observed but was significantly lower than specific binding (Fig. 1*A*).

From the binding data, the K_d and the maximum number of liposomes bound/cell were determined. The number of liposomes/μmol PL was estimated to be 7.7×10^{12} liposomes/μmol PL (calculated from the literature values for bilayer thickness and the molecular areas of PL, CHOL, and PEG, with the assumptions that liposomes were spherical, 100 nm in diameter, monodisperse, and contained unilamellar bilayers; Refs. 61–65). This translates into approximately 48,000 total binding sites for $CD19^+$ Namalwa cells by SIL[anti-CD19] (*versus* 15,000 SL nonspecifically bound) at saturated concentrations of PL. Therefore, there are 33,000 specific binding sites for SIL[anti-CD19] on Namalwa cells. The K_d for the SIL[anti-CD19] was 160 μM PL, which was 2.5-fold greater than than seen for the SL.

The binding/uptake of SIL[anti-CD19] by the $CD19^-$ T-cell line H9 was significantly lower than that for the $CD19^+$ B cells, and no significant differences were observed in comparison with control Ab-free liposomes (Fig. 1*C*). Binding/uptake of SIL[anti-CD19] to Namalwa cells at 37°C was significantly higher than the binding at 4°C (Fig. 1, *A versus B*), suggesting a requirement for metabolic processes in the uptake of SIL[anti-CD19] by the target cell (66).

Specific Recognition of Immunoliposomes SIL[anti-CD19] to B Cells in a Mix of B Cells and T Cells. Using flow cytometry (FACS) and green fluorescent NBD-liposomes, specific labeling to human B-cell lymphoma (the Namalwa cell line) was evaluated in a mix of $CD19,20^+$ Namalwa and $CD4^+CD19^-$ T-cell lines (Fig. 2). Fig. 2*A* shows cells stained with isotype-matched control Abs. In Fig. 2*B*, after staining with fluorescent mAb anti-CD19-FITC (B cells) and anti-CD4-PhE (T cells), the mixture of cells could be resolved into two populations containing 44% of the $CD19^+$ B cells and 47% of the $CD4^+$ T cells, respectively. Treatment with nontargeted SLs showed no appreciable association of the NBD green fluorescence to either the $CD20^+$ B cells (Fig. 2*C*) or the $CD4^+$ T-cell population (Fig. 2*D*). On the other hand, SIL[anti-CD19] selectively bound B cells (Fig. 2*E*) in which 40% of the cells were dual-labeled with SIL[anti-CD19] (green fluorescence) and CD20-PhE (red fluorescence), as seen in the *upper right quadrant* of Fig. 2*E*, with the rest of the cells almost exclusively unstained (presumably $CD20^-$ T cells). To confirm the identity of this unstained population (presumably T cells), cells were stained with T-cell marker anti-CD4-PhE after treatment with SIL[anti-CD19] (Fig. 2*F*). In this case, the cell mixture was again separated into two distinct populations (Fig. 2*F*). Cells (47%) were either exclusively $CD4\text{-PhE}^+$ (Fig. 2*F*, *lower right*) with low NBD fluorescence (*i.e.*, no association of targeted liposomes with T cells) or $CD4^-$ cells that were labeled (33%) SIL[anti-CD19] (Fig. 2*F*, *upper left*; *i.e.*, $CD4^-$ B cells). Only a small proportion of cells (12% or less) seemed dual-labeled with both NBD and CD4-PhE seen in the upper right quadrant). In comparison, neither SL (Fig. 2, *C* and *D*) nor NSIL[IgG2a] (data not shown) bound any of the cells.

***In Vitro* Cytotoxicity of SIL[anti-CD19].** The cytotoxicity of DXR-SIL[anti-CD19], DXR-SL, free DXR, free mAb, and drug-free controls were compared as a function of time. As seen in Table 1, the IC_{50} decreased as the exposure of cells to drug increased from 1 h to 48 h. After a 1-h incubation, targeted DXR-SIL[anti-CD19] was 6-fold more cytotoxic than nontargeted liposomes ($P < 0.001$) or isotype-matched liposomes DXR-NSIL[IgG2a] ($P < 0.001$) for the Namalwa cell line. This suggests that binding and/or internalization of the targeted liposomes are contributing to the increased cytotoxicity. Whereas DXR-SIL[anti-CD19] displayed a cytotoxicity approaching that of the free DXR ($P > 0.05$), both nontargeted liposomal formulations were significantly less cytotoxic than the free DXR *in vitro* ($P < 0.001$). With incubations of 24 and 48 h, the difference in cytotoxicity between DXR-SL and DXR-SIL[anti-CD19] decreased 4-fold ($P < 0.01$; Table 1). This likely results from the gradual release of the encapsulated drug from the DXR-SL with uptake of the released drug with longer incubation times. When the cytotoxicities were compared on the $CD19^-$ H9 T-cell line, no significant differences were observed in the IC_{50} of DXR-SIL[anti-CD19] compared with nontargeted DXR-SL both at 1 and 24 h ($P > 0.05$), suggesting the requirement of CD19 receptors in mediating cytotoxicity of targeted DXR-SIL[anti-CD19]. Free DXR demonstrated a 3-fold greater cytotoxicity to B cells (Namalwa), compared to the T-cell line (H9; $P < 0.05$; Table 1). However, the cytotoxic effects of the liposomal formulations to T cells *versus* B cells were reversed. The liposomal-DXR formulations were 1.5–2-fold less cytotoxic to B cells in comparison to T cells ($P < 0.01$) at 1- and 24-h incubations (Table 1). Because cytotoxicity is mediated by DXR released from liposomes, this suggests that the T-cell preparations may increase leakage of the drug from DXR-SL.

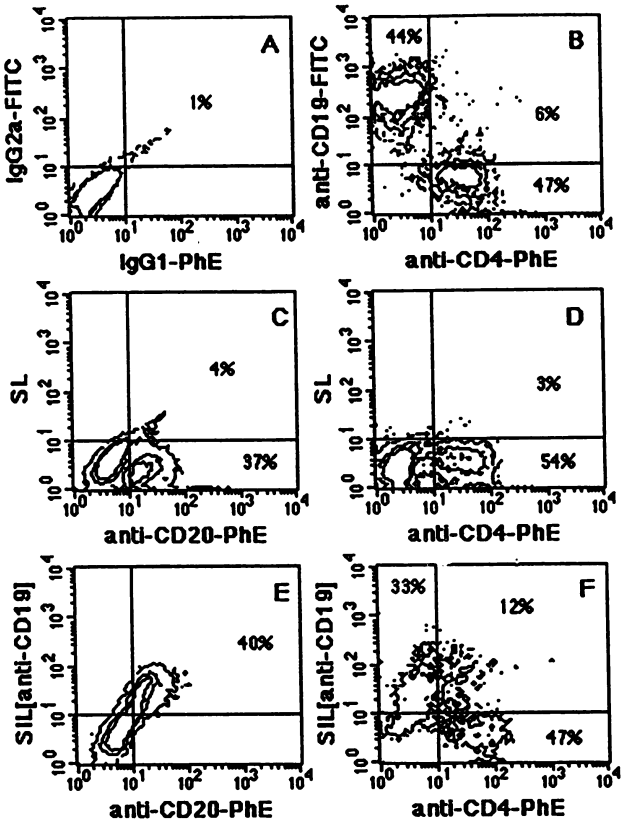

Fig. 2. Two-color flow cytometry for selective recognition of fluorescent NBD-labeled liposomes by $CD19^+$ B lymphoma cells (Namalwa). NBD-labeled (0.1 mol% of PL) liposomes were composed of HSPC:CHOL:PEG_{2000}-DSPE (2:1:0.1 molar ratio; 100 nm in diameter) ± mAb anti-CD19. A mixture of $CD19,20^+$ B cells and $CD4^+$,$CD19^-$ T cells was incubated with either SIL[anti-CD19] or SL and stained with either anti-CD20-PhE (B1RD1, B-cell marker) or anti-CD4-PhE (T-cell marker). *A*, cells stained with the appropriate fluorescent isotype-matched control Abs; *B*, mAbs anti-CD19-FITC and anti-CD4-PhE; *C*, SL and anti-CD20-PhE; *D*, SL and anti-CD4-PhE; *E*, SIL[anti-CD19] and anti-CD20-PhE; *F*, SIL[anti-CD19] and anti-CD4-PhE.

Additional control experiments were performed to rule out the possibility that the cytotoxic effect may arise from either the lipid, mAb, or a combination of both. Free mAb (anti-CD19) molecules were, on a molar basis, equivalent in cytotoxicity to free DXR molecules ($P > 0.05$; Table 1). The isotype-matched control IgG2a

Table 1 *Cytotoxicity data (IC_{50}) for free anti-CD19, isotype-matched control mAb, SILs, free DXR, and DXR-liposomal formulations (with or without anti-CD19) determined on $CD19^+$ B cells (Namalwa) and $CD19^-$ T lymphoma (H9) cells by the MTT assay*

Five × 10^5 cells were plated in 96-well plates and incubated with either free DXR or various formulations of DXR encapsulated in long-circulating liposomes with or without Ab. Groups included free anti-CD19, isotype-matched control mAb IgG2a, free DXR, DXR-SL, DXR-SL conjugated to either anti-CD19 (DXR-SIL[anti-CD19]; alone or in conjunction with free anti-CD19; 10 μg/10^6 cells) or nonspecific isotype-matched IgG2a mAb (DXR-NSIL[IgG2a]), and drug-free SIL[anti-CD19]. Ab coupling via the PEG-Hz method was 40–50 μg mAb/μmol PL (2.6–3.9 × 10^{-4} μmol mAb/μmol PL), and DXR loading was 140–160 μg DXR/μmol PL (0.24–0.28 μmol DXR/μmol PL). Cells were incubated for 1 or 24 h at 37°C in an atmosphere of 95% humidity and 5% CO_2. At the end of each incubation period, cells were washed twice before replacing with fresh media. Plates were incubated for a total of 48 h, tetrazolium dye (50) was added, and the plates were read at dual wavelengths of 570 and 650 nm. Cytotoxicity data are expressed as mean IC_{50} ± SD (n = 2–7).

	Free mAb anti-CD19 (μM)	Free mAb isotype-matched IgG2a (μM)	Drug-free SIL[anti-CD19] (μM PL)	Free DXR (μM DXR)	anti-CD19 + free DXR (μM DXR)	DXR-SL (μM DXR)	anti-CD19 + DXR-SL (μM DXR)	DXR-NSIL [IgG2a] (μM DXR)	DXR-SIL [anti-CD19] (μM DXR)	anti-CD19 + DXR-SIL [anti-CD19] (μM DXR)	IC_{50} ratio DXR-SL:DXR-SIL [anti-CD19]
Namalwa cells											
1 h	1.00 ± 0.04	>2.6	>1500	1.30 ± 0.6	0.79 ± 0.10	78.1 ± 14.0	139.7 ± 21.2	67.1 ± 11.2	13.5 ± 9.8	55.9 ± 13.3	5.8:1
24 h	0.43 ± 0.10	>2.6	230 ± 30	0.28 ± 0.1	0.22 ± 0.05	5.1 ± 1.4	1.4 ± 0.4	10.9 ± 3.1	1.4 ± 1.2	3.32 ± 0.86	3.6:1
48 h				0.07 ± 0.01		4.4 ± 0.4		5.0 ± 0.6	1.2 ± 0.1		3.7:1
H9 cells											
1 h				3.2 ± 1.0		30.5 ± 8.0			38.5 ± 22.4		0.8:1
24 h				0.76 ± 0.6		1.5 ± 0.7			1.9 ± 0.9		0.8:1

was not cytotoxic in the concentration range tested (Table 1). Drug-free liposomes, which contain approximately 3.2 × 10^{-4} μmol Ab/μmol PL, did not seem to have significant cytotoxicity (Table 1).

Coincubation of free anti-CD19 at concentrations found on the mAb-coupled liposomes with free DXR did not significantly alter the IC_{50} of the free drug ($P > 0.05$); hence, low concentrations of anti-CD19 do not seem to sensitize Namalwa cells to free drug *in vitro*. Anti-CD19 incubated with DXR-SL had minimal effects on cytotoxicity at 1 or 24 h ($P < 0.05$). Free anti-CD19 competed with DXR-SIL[anti-CD19] and increased the IC_{50} of the targeted liposomes by 4-fold after a 1-h incubation ($P < 0.01$), giving an IC_{50} that was not significantly different from that of nontargeted DXR-SL or DXR-NSIL[IgG2a] ($P > 0.05$). No competition effect of free anti-CD19 for DXR-SIL[anti-CD19] was observed at 24 h (Table 1).

Table 2 *Summary of tumor dissemination of human B-cell lymphoma (Namalwa cells) after i.p. and i.v. implantation in SCID mice*

	Route of implantation of Namalwa cells	
	i.p. (5 × 10^7 cells)	i.v. (5 × 10^6 cells)
MST	23.4 ± 2.7 days	20.4 ± 1.6 days
End point	Ascitic tumor	Hind leg paralysis
Blood	++[a]	−
Ascites development	+++	−
Liver	++	++
Spleen	++	++
Lung	+	++
Solid tumors in the lymph nodes	+++	++
Bone marrow	−	+++
Hind leg paralysis	−	+++

[a] Relative levels of implantation of cells in mice after histological examination. +++, high; ++, intermediate; +, low; or −, no cells identified in tissue sections.

Tumor Model of Namalwa Cells Implanted in SCID Mice. After i.p. injection, mice implanted with Namalwa cells developed an ascitic tumor accompanied by an approximately 30% gain in body weight. At necropsy, the tumor was found to have invaded the blood and lymph nodes (particularly the mesenteric lymph nodes and serosal surfaces) with disseminated involvement of the liver, spleen, diaphragm, anterior thoracic cavity, lungs, ovaries, and heart (pericardium; Table 2). After i.v. injection of the cells, the primary tissues of infiltration were lymph nodes, bone marrow, spleen, lung, liver, and renal capsule (Table 2). In contrast to the i.p. model, there were no significant numbers of tumor cells found circulating in the blood at 24 h after inoculation when treatment began. When hind leg paralysis was observed after i.v. implantation as a result of cells infiltrating the vertebrae and compressing the spinal cord, the mice were sacrificed.

Cell surface expression of CD19 was examined in SCID mice implanted with Namalwa cells. FACS analysis demonstrated that the *in vivo* transplantation of these cells did not result in a significant variation of CD19 surface antigen expression in tissues. Compared with cells in culture, CD19 expression seemed slightly depressed in solid tumors, particularly in the lymph nodes. Cells isolated from solid tumors regained surface expression of CD19 when they were returned to culture. To examine the tumor dissemination after i.p. or i.v. implantation, dissociated cells from excised tissues were retrieved and stained with both anti-CD19 and anti-CD45. The additional staining with anti-CD45 was done to identify human leukocytes, to discrimi-

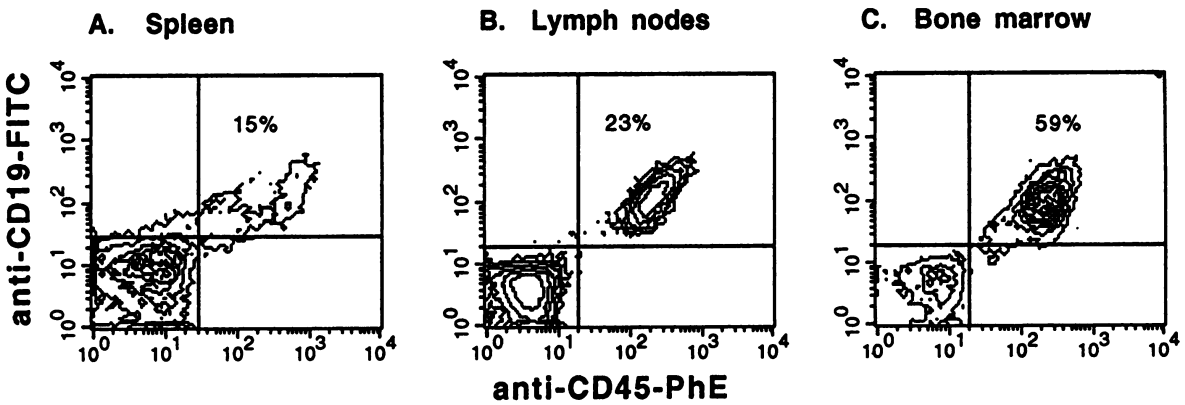

Fig. 3. Two-color flow cytometry to determine the degree of implantation of Namalwa cells in various tissues after i.v. implantation in SCID mice. Dissociated cells from the excised tissues were stained with both anti-CD19-FITC (human B-cell marker) and human anti-CD45-PhE (common leukocyte antigen marker). *A*, spleen; *B*, lymph nodes; *C*, bone marrow.

DOCKET ALARM

Explore Litigation Insights

Docket Alarm provides insights to develop a more informed litigation strategy and the peace of mind of knowing you're on top of things.

Real-Time Litigation Alerts

Keep your litigation team up-to-date with **real-time alerts** and advanced team management tools built for the enterprise, all while greatly reducing PACER spend.

Our comprehensive service means we can handle Federal, State, and Administrative courts across the country.

Advanced Docket Research

With over 230 million records, Docket Alarm's cloud-native docket research platform finds what other services can't. Coverage includes Federal, State, plus PTAB, TTAB, ITC and NLRB decisions, all in one place.

Identify arguments that have been successful in the past with full text, pinpoint searching. Link to case law cited within any court document via Fastcase.

Analytics At Your Fingertips

Learn what happened the last time a particular judge, opposing counsel or company faced cases similar to yours.

Advanced out-of-the-box PTAB and TTAB analytics are always at your fingertips.

API

Docket Alarm offers a powerful API (application programming interface) to developers that want to integrate case filings into their apps.

LAW FIRMS
Build custom dashboards for your attorneys and clients with live data direct from the court.

Automate many repetitive legal tasks like conflict checks, document management, and marketing.

FINANCIAL INSTITUTIONS
Litigation and bankruptcy checks for companies and debtors.

E-DISCOVERY AND LEGAL VENDORS
Sync your system to PACER to automate legal marketing.